Chapter 14

CHROMATIN SIMULATIONS

From DNA to chromatin fibers

J. Langowski and H. Schiessel

[1]*Division Biophysics of Macromolecules, German Cancer Research Center (DKFZ), Im Neuenheimer Feld 580, D-69120 Heidelberg, Germany*

[2]*Instituut-Lorentz, Universiteit Leiden, P.O. Box 9506, 2300 RA Leiden, The Netherlands*

Abstract: We give an overview over current coarse-grained models of DNA and the chromatin fiber. A short review of the major structural elements, interaction potentials and mechanical parameters relevant for chromatin structure is given. We then discuss the role of histone tails in nucleosome-nucleosome interaction and finally report some new results on the simulation of chromatin stretching by analytical and numerical models.

Key words: wormlike polymer chain, persistence length, Monte-Carlo models, Brownian dynamics, elasticity theory, single molecule stretching, nucleosome unrolling

1. INTRODUCTION

The genomic DNA and the histone proteins compacting it into chromatin comprise most of the contents of the nucleus. In every human cell, for instance, $6 \cdot 10^9$ base pairs of DNA – that is, a total length of about 2 meters – must be packed into a more or less spheroid nuclear volume about 10-20 μm in diameter. This compaction must occur in such a way that the DNA molecule is still easily accessible to enzymes acting on it, such as replication, transcription and repair machineries, or regulatory factors.

Figure 1 gives an overview of the many length and time scales that have to be considered to describe DNA compaction. Describing such a complex system with molecular dynamics methods that have been successful in modeling medium-size proteins and protein-DNA complexes would be

impossible with present computational means and not even desirable (in fact, such an undertaking would be almost comparable to predicting the weather by solving the equations of motion of all the water molecules in the atmosphere). Thus, such a system must be described using some adequate

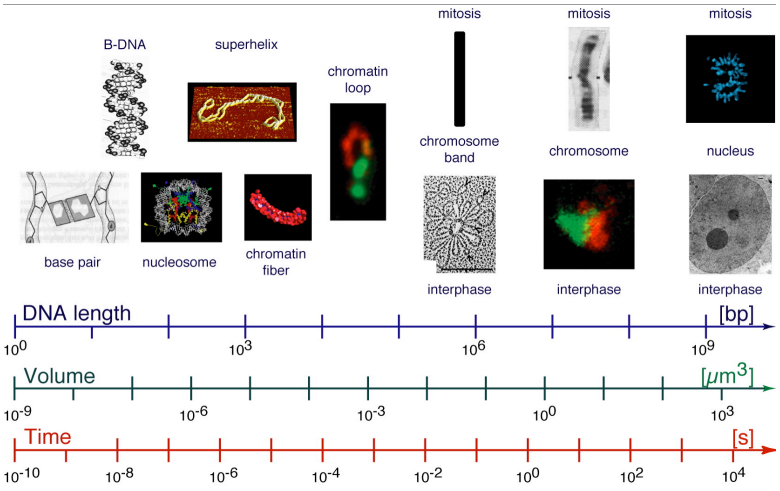

Fig. 1: Time and length scales relevant in genome organization.

approximation.

The principle of any such approximation will consist in defining suitable subunits of the molecule that behave like rigid object on the size and time scale considered. These objects interact through potentials that may in principle be derived from the interatomic force fields; however, in practice one mostly uses potentials that have been determined experimentally. To derive general principles of DNA and chromatin structure and dynamics, some models can be described analytically by closed equations; in many other cases, however, the potentials and the mechanics involved are more complicated and numerical simulations must be applied. Examples of both approaches will be given here.

The lowest level of DNA compaction in eukaryotic cells is the chromatin fiber: 147 bp stretches of DNA, which are wrapped in 1.65 left-handed turns about histone octamers formed by two copies each of the histones H2A, H2B, H3 and H4, alternate with free linker DNAs of 20-80 bp length. This repeating unit of the chromatin fiber is called the nucleosome; the histone octamer, together with the bound DNA, is the nucleosome core particle (NCP). The structure of the NCP has been determined by X-ray crystallography to atomic resolution[1-3]. At low ionic strengths, the polynucleosome chain forms a zig-zag, 'bead-on-a-string' structure (10 nm

fiber), clearly seen on micrographs obtained by cryoelectron microscopy. Under physiological ionic conditions, the chromatin is more condensed (30 nm fiber). Its detailed structure in this state is yet unknown, however, recently the first high resolution crystallographic structure of a tetranucleosomes was published[4].

Two classes of models were proposed for the arrangement of NCPs inside the 30 nm fiber: the solenoid models[5-7] and the zig-zag models[8-13]. According to the solenoid model, the NCPs are packed one by one along a solenoid helix in the same order as they follow in the chain. The linker DNA is bent in order to provide a relatively small distance between the neighboring NCPs. On the contrary, in the zig-zag model, straight linkers connect the NCPs located on opposite sides of the fiber. The NCPs are also arranged in a helical order, but the neighbors in space are the second neighbors along the chain. Most recent experimental data on chromatin fibers[9,11,12,14-16], as well as the tetranucleosome crystallographic structure[4], are rather in favor of the zig-zag model, which is also energetically more favorable because the linker DNA does not need to bend.

The regular fiber geometry of the zig-zag model can be quantitatively described in terms of two parameters: the entry-exit angle α of the linker DNAs at each NCP and the twist angle β between successive NCPs on the chain. Therefore, in theoretical considerations, this model is often referred to as the two-angle model[13]. The angle α is strongly influenced by the linker histone (H1 or H5) located near the entry-exit region of the NCP. Through the DNA helix pitch, the angle β is coupled with the linker DNA length.

In reality, the 30 nm fiber structure is not quite so regular. It suffers transient fluctuations due to thermal motion. Statistical and dynamical properties of such a complex system can be understood only by means of numerical simulations. Because of the size of the system, standard all-atom molecular dynamics techniques that are successful for describing small and intermediate size biomolecules are not adequate. In order to deal with a system as large as the nucleosome or beyond, it must be appropriately ‘coarse-grained’, that is, groups of atoms must be comprised into larger units that are interacting via effective potentials. In recent years, several works dedicated to computer simulations of the 30 nm fiber were published[13,17-23]. In those works, the NCP was modeled by a sphere, an oblate ellipsoid, or a disk and the linker DNA was considered as a chain of straight segments with elastic joints. The "coarse-grained" energy defined in these systems was essentially based on the two-angle model, with α and β being adjustable parameters, on the known flexibility parameters of DNA and on reasonable assumptions for the internucleosome interaction.

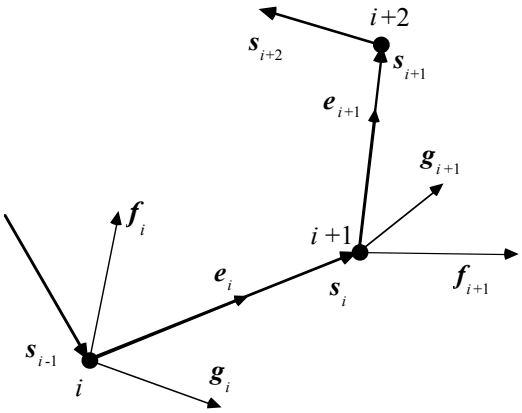

Fig. 2: Section of a segmented polymer chain as used in the DNA and chromatin models described here.

2. COARSE-GRAINED MODELS OF DNA

For setting up a model of the chromatin fiber, we must first be able to describe the mechanics of a long DNA chain. A 'coarse-grained' description of DNA can be achieved using a linear segmented chain. We see in Fig. 1 that the motif of a 'linear elastic filament' is repeated through all size scales: DNA, as well as the chromatin fiber and to some extent its higher order structures may be approximated by a flexible wormlike chain. An approximate description for such a molecule is constructed by defining suitable segments, which behave like rigid cylinders on the time and length scale considered. Fig. 2 schematizes the segmented chain geometry. The vector $\mathbf{s}_i$ defines the direction and length of segment i, $\mathbf{f}_i$ is a unit vector normal to the segment and $\mathbf{g}_i$ is an auxiliary vector that is used to take into account permanent bending of the DNA. The details of this chain geometry are given in [24].

2.1 DNA flexible wormlike chain – nanomechanical parameters

Neglecting all structural detail, four parameters are sufficient to describe the energetics of the segmented chain: elastic constants for bending, torsion

and stretching and the interaction potential between chain segments (the latter also relating to the thickness of the molecule).

2.1.1 Bending rigidity

The length of the segments must be chosen well below the *persistence length* L_p, which is a measure of the bending flexibility of the chain molecule. It is defined as the correlation length of the direction of the chain measured along its contour:

$$\left\langle \vec{u}(s)\vec{u}(s+s')\right\rangle = e^{-s'/L_p} \qquad (1)$$

Here $\vec{u}(s)$ is a unit vector in the direction of the chain ($\boldsymbol{e}_i$ in Fig. 2) and s resp. $s+s'$ are the positions along the chain contour, the angular brackets indicating the thermal average over all positions and chain conformations. Molecules shorter than L_p behave approximately like a rigid rod, while longer chains show significant internal flexibility. The bending elasticity A – the energy required to bend a polymer segment of unit length over an angle of 1 radian – is related to the persistence length by $L_p = A/k_BT$, k_B being Boltzmann's constant and T the absolute temperature. The energy required to bend two segments of the chain of length l by an angle θ with respect to one another is:

$$E_b = \frac{k_BT}{2}\frac{L_p}{l}\theta^2 \qquad (2)$$

For DNA, L_p has been determined in a number of experiments (for a compilation, see [25]). While some uncertainties remain as regards the value at very high or low salt concentrations, the existing data agree on a consensus value of L_p = 45-50 nm (132-147 bp) at intermediate ionic strengths (10-100 mM NaCl and/or 0.1-10 μM Mg^{2+}).

2.1.2 Torsional rigidity

The torsional rigidity C, defined as the energy required to twist a polymer segment of unit length through an angle of 1 radian, may be related in an analogous way to a *torsional persistence length* L_T through the directional correlation of a vector normal to the chain axis and with fixed orientation relative to the molecular structure of the polymer chain (e.g. for DNA one would use a vector pointing along the dyad axis for the first base pair and into a direction of $(n-1)\times 360°/10.5$ to the left of the dyad axis for the n-th base pair, assuming a helix period of 10.5 base pairs per turn). Again, C is

related to L_T by $L_T = C/k_BT$ and the torsion energy between two segments of length l twisted by an angle ϕ:

$$E_T = \frac{k_B T}{2} \frac{L_T}{l} \phi^2 \qquad (3)$$

The torsional rigidity C has been measured by various techniques, including fluorescence polarization anisotropy decay [26-28] and DNA cyclization [29-31], and the published values converge on a torsional persistence length of 65 nm (191 bp).

2.1.3 Stretching rigidity

The stretching elasticity of DNA has been measured by single molecule experiments [32,33] and also calculated by molecular dynamics simulations [34,35]. The stretching modulus σ of DNA is about 1500 pN, where $\sigma = F \cdot L_0 / \Delta L$ (ΔL being the extension of a chain of length L_0 by the force F). The stretching energy of a segment of length l that is stretched by Δl is:

$$E_{str} = \frac{1}{2} \frac{\sigma}{l} \Delta l^2 \qquad (4)$$

DNA stretching probably does not play a significant role in chromatin structural transitions, since much smaller forces are already causing large distortions of the 30 nm fiber (see below).

2.1.4 Intrachain interactions

The average DNA helix diameter used in modeling applications such as the ones described here includes the diameter of the atomic-scale B-DNA structure and – approximately – the thickness of the hydration shell and ion layer closest to the double helix[36]. Both for the calculation of the electrostatic potential and the hydrodynamic properties of DNA (i.e. the friction coefficient of the helix for viscous drag) a helix diameter of 2.4 nm describes the chain best[24,37-39]. The choice of this parameter is supported by the results of chain knotting[40] or catenation[41], as well as light scattering[42] and neutron scattering [39] experiments.

As pointed out in[24,43] DNA intrachain electrostatic repulsion can be adequately described by a Debye-Hückel electrostatic potential between two uniformly charged non-adjacent segments (i, j) in a 1-1 salt solution:

$$E_{ij}^{(e)} = \frac{\nu^2}{D} \iint d\lambda_i d\lambda_j \frac{e^{-\kappa r_{ij}}}{r_{ij}} \qquad (5)$$

Here, the integration is done along the two segments, λ_i and λ_j are the distances from the segment beginnings, r_{ij} is the distance between the current positions at the segments to which the integration parameters λ_i and λ_j correspond; κ is the inverse of the Debye length, so that $\kappa^2 = 8\pi e^2 I / k_B T D$, I is the ionic strength, e the proton charge, D the dielectric constant of water, ν the linear charge density which for DNA is equal to $\nu_{DNA} = -2e/\Delta$ where Δ = 0.34 nm is the distance between base pairs. More details as to the normalization of the linear charge density etc. have been given in our earlier paper [24].

3. SIMULATION PROCEDURES

3.1 Monte-Carlo simulations

The total energy of a segmented polymer chain is given by the sum of bending, twisting, stretching and intrachain interaction energies (eqs. 2-5):

$$E_{total} = E_b + E_T + E_{str} + E^{(e)} \qquad (6)$$

To find a realistic chain conformation, one could now search for the conformation of minimum energy. Caution must be taken, however, that a simple search for the minimum of elastic energy will not be enough, because the system is highly degenerate: at equilibrium there exist a large number of possible conformations whose energy differs by much less than the thermal energy k_BT [44].

An ensemble of configurations at thermodynamic equilibrium, i.e. at minimum *free* energy, can be produced by the Metropolis Monte-Carlo algorithm [45]: Starting from a configuration i with Energy E_i, we generate configuration $i+1$ by a small statistical variation, e.g., by translating or rotating a group of atoms in the molecule. The new energy E_{i+1} is then calculated; the new configuration is counted into the average and taken as the new starting configuration if either $E_{i+1} < E_i$ or $X < e^{-(E_{i+1}-E_i)/k_BT}$, where $X \in [0,1]$ is a uniformly distributed random number. Otherwise the configuration i is counted again into the average. It can be shown that this procedure generates an ensemble of configurations of the molecule at thermodynamic equilibrium at temperature T.

For the DNA chain, a typical statistical variation (or 'Monte Carlo move') might be for instance a rotation of part of the molecule around a randomly taken axis. The characteristics of Monte Carlo procedures are described in more detail in the original papers such as [37,46].

3.2 Brownian dynamics simulations

For calculating the dynamics of DNA, equations of motion for the segmented DNA chain have to be set up using the intramolecular interaction potentials described above and including the thermal motion through a random force. This is the Brownian Dynamics (BD) method [47] which several groups applied to DNA in interpreting experimental data from fluorescence depolarization [48], dynamic light scattering [49,50], or triplet anisotropy decay [51]. Superhelical DNA has also been modeled by a BD approach [52,53]. The model allows to predict the kinetics of supercoiling and the internal motions of superhelical DNA over a time range of tens of milliseconds. This model has then been used in extensive studies of intramolecular reactions in superhelical DNA [54-58].

In the model, the equations of motion of a polymer chain of N segments in a viscous fluid are iterated numerically with a time step δt. The discrete equations of motion in the solvent for positions $\mathbf{r}_i$ and torsions ϕ_i of the i-th segment are then [59]:

$$\begin{aligned} \delta\mathbf{r}_i(t) &= \delta t \frac{1}{k_B T} \sum_{j=1}^{N} \mathbf{D}_{ij}\mathbf{F}_j + \mathbf{R}_i \\ \delta\phi_i(t) &= \delta t \frac{1}{k_B T} D_r T_i + S_i \end{aligned} \qquad (7)$$

where $\mathbf{D}_{ij}$ is a *hydrodynamic* interaction *matrix* (see below), D_r is the rotational diffusion coefficient (same for all segments), $\mathbf{F}_j$ and T_i are the forces and torques acting on segment j resp. i, and the random translations $\mathbf{R}_i$ and rotations S_i are sampled from Gaussian distributions with the following properties:

$$\begin{aligned} \langle \mathbf{R}_i \rangle = 0 \quad ; \quad \langle \mathbf{R}_i : \mathbf{R}_j \rangle = 2\delta t \mathbf{D}_{ij} \\ \langle S_i \rangle = 0 \quad ; \quad \langle S_i S_j \rangle = 2\delta t D_r \end{aligned} \qquad (8)$$

The (3N x 3N) $\underline{\mathbf{D}}_{ij}$ matrix in the first line of Eqs.7,8 is the Rotne-Prager generalization of the Oseen tensor [60], which characterizes the hydrodynamic interaction between two spherical beads (eq. 5 and 6 in Chirico and Langowski [50]) For calculation of this matrix, the cylindrical DNA segments are approximated by beads with radius r_b = 2.53 nm. The model has been

described in detail in several papers [24,50,52,61], and its code is available on request from the author.

4. NUCLEOSOMES

4.1 Nucleosome structure

As mentioned above, the structure of the nucleosome core particle is known in detail from X-ray crystallography [1,2]. The histone octamer defines the wrapping path of the DNA, a left-handed helical ramp of 1 and 3/4 turns, 147 bp length and a ~28 Å pitch. This aggregate has a two-fold axis of symmetry (the dyad axis) that is perpendicular to the DNA superhelix axis. A schematic view of the NCP is given in Fig. 3.

The regions where the wrapped DNA contacts the octamer surface are located where the minor grooves of the right-handed DNA double helix face inwards towards the surface of the octamer. There are 14 'sticking points' on the octamer surface, and while structural details for them are known, a reliable quantitative estimate of the free energy of binding per sticking point is still missing.

From studies of competitive protein binding to nucleosomal DNA[62,63] the adsorption energy per sticking point is estimated at $\sim 1.5 - 2 k_B T$. This number has to be taken with a grain of salt; first, it does not represent the *pure* adsorption energy but instead the *net* gain in energy that is left after the DNA has been bent around the octamer to make contact to the sticking point. A rough estimate of the deformation energy can be obtained from the DNA

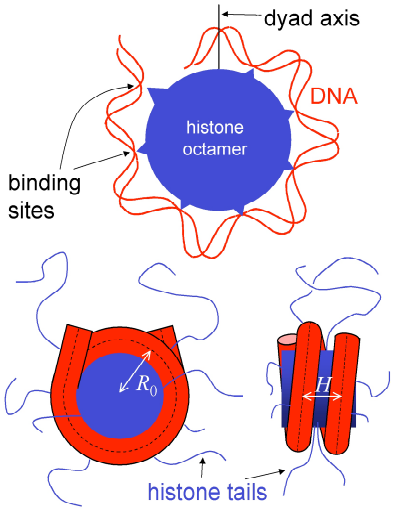

Figure 3. The top picture displays only the upper half of the wrapped DNA with its binding points to the histone octamer (located at the positions where the minor groove faces the octamer). At the bottom the full NCP is shown from the top and from the side. Also indicated are the 8 histone tails.

persistence length L_P of ~50 nm. Then the elastic energy required to bend the 127 bp of DNA around the octamer (10 bp at each terminus are essentially straight [1]) is given by

$$\frac{E_{elastic}}{k_B T} = \frac{L_P l}{2R_0^2} \qquad (9)$$

Here l is the bent part of the wrapped DNA, $\sim 127 \times 3.4$ Å $= 432$ Å and R_0 is the radius of curvature of the centerline of the wrapped DNA that is roughly 43 Å [1]. This leads to a bending energy of order $58 k_B T$, a number, however, that has again to be taken with caution since it is not clear whether the assumption of a homogeneous elastic filament holds up to such strong curvatures. Using these numbers nevertheless one can estimate the bending energy per ten basepairs, i.e., per sticking site, to be of order $60 k_B T / 14 \approx 4 k_B T$ [64].

Together with the observation that the net gain per sticking point is $\sim 2 k_B T$ this means that the pure adsorption energy is on average $\sim 6 k_B T$ per binding site. Note that the huge pure adsorption energy of $\sim 6 k_B T \times 14 \approx 85 k_B T$ per nucleosome is cancelled to a large extend by the $\sim 58 k_B T$ from the DNA bending, a fact that has important consequences for nucleosomal dynamics.

4.2 Nucleosome unwrapping – analytical model

As has been shown experimentally in several cases, for large enough external stretching forces the DNA unwraps from the octamer and the nucleosome falls apart. It seems to be straightforward to estimate the critical force necessary to induce such an unwrapping from the net adsorption energy of the 50 nm DNA wrapped in the nucleosome, about $30 k_B T$:

$$F_{crit} \approx \frac{30 k_B T}{50 nm} = 2.5 pN \qquad (10)$$

The same critical force should be expected if there are several nucleosomes associated with the DNA fragment; all of them should unwrap at the same critical force. However, a recent experiment[65] on reconstituted chromatin fibers resulted in unwrapping forces very different from what Eq. (10) predicts. The experiment was performed on tandemly repeated nucleosome positioning sequences with up to 17 nucleosomes complexed at well-defined positions. When small forces ($F < 10 pN$) were applied for short times ($\sim 1 - 10 s$) the nucleosome unwrapped only partially by releasing the outer 60-70 bp of wrapped DNA in a gradual and equilibrium fashion. For higher forces ($F > 20 pN$) nucleosomes showed a pronounced sudden

non-equilibrium release behavior of the remaining 80 bp – the latter force being much larger than expected from the above given equilibrium argument. To explain this peculiar finding Brower-Toland et al. [65] conjectured that there must be a barrier of $\sim 38 k_B T$ in the adsorption energy located after the first 70-80 bp and smeared out over not more than 10 bp which reflects some biochemical specificity of the nucleosome structure at that position. However, there is no experimental indication of such a huge specific barrier – neither from the crystal structure [2] nor from the equilibrium accessibility to nucleosomal DNA[62]. Kulic and Schiessel [66] argued that the barrier is caused by the underlying geometry and physics of the DNA spool rather than by a specific biochemistry of the nucleosome.

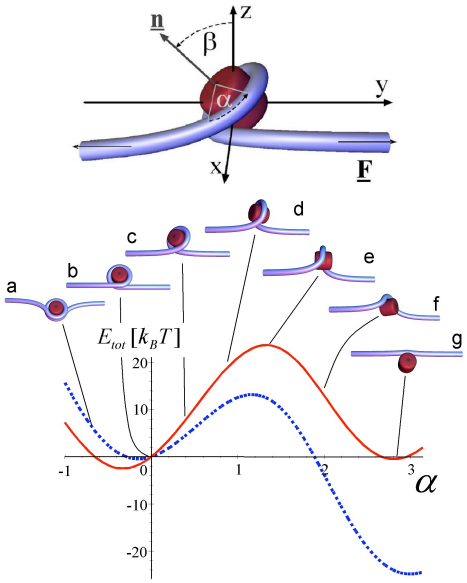

Figure 4. A nucleosome under tension. The top picture defines the two angles involved in the unwrapping process: the desorption angle α and the tilting angle β. The bottom shows the nucleosome unwrapping that involves a 180°-rotation of the octamer and the associated energy, Eq.(13), as a function of α for an applied tension of 6.5 pN. Unwrapping is only possible as an activated process going across a substantial barrier.

Summarizing the arguments in that work, we show in Fig. 4 the model of a DNA spool under tension. The elastic energy of a WLC of length L is

$$E_{bend} = \frac{A}{2}\int_0^L ds\,\kappa^2(s) \qquad (11)$$

with $\kappa(s)$ being the curvature of the chain at point *s* along its contour (this is the continuum version of Eq. (2)). The DNA is assumed to be adsorbed on the protein spool surface along the predefined helical path with radius R_0 and pitch height *H*, with a pure adsorption energy density per wrapped length, k^a, given by the pure attraction of the binding sites (not including the bending contribution).

The degree of DNA adsorption is described by the desorption angle α which is defined to be zero for one full turn wrapped (cf. top of Fig. 4). During unwrapping the spool needs to rotate transiently out of the plane while performing a full turn – as already pointed out by Cui and Bustamante[67]. Therefore a second angle, β, is introduced to describe the out-of-plane tilting of the spool, cf. Fig. 4. When a tension *F* (along the *Y*–axis) acts on the two outgoing DNA arms the nucleosome will simultaneously respond with DNA deformation, spool tilting and DNA desorption from the spool.

The total energy of the system as a function of α and β has three contributions:

$$E_{tot}(\alpha,\beta) = E_{bend} + 2R_0 k^a \alpha - 2F\Delta y \qquad (12)$$

The first term in Eq. (12) is the deformation energy of the DNA chain, Eq. (11), the second describes the desorption cost and the third term represents the potential energy gained by pulling out the DNA ends, each by a distance Δy.

It is possible to work out the total energy on purely analytical grounds by calculating the shape and energy of the DNA arms accounting for the right boundary conditions at the points where the DNA enters and leaves the spool and at the DNA termini (that are assumed to be far from the spool). Instead of giving the full analytical expression of E_{tot} provided in Kulic and Schiessel [66], we merely present here a reasonable approximation in the limit for a flat spool with $R_0 \gg H$ and setting $\alpha = \beta$. In this case

$$\begin{aligned} E_{tot}(\alpha) \approx\ & 2R\left[k^a - \frac{A}{2R_0^2} - F\right]\alpha + 2FR\cos\alpha\sin\alpha \\ & + 8\sqrt{AF}\left[1 - \sqrt{(1+\cos^2\alpha)/2}\right] \end{aligned} \qquad (13)$$

In Fig. 4 we plot the resulting energy landscape for a force of $F = 6.5$ pN. The dashed curve corresponds to the value $k^a = 2k_BT/nm$ as inferred from competitive protein binding data (see section 4.1); for the thick curve we assume a larger value, $k^a = 3k_BT/nm$ (see below).

4.3 Brownian dynamics simulation of nucleosome unwrapping

A similar unwrapping barrier as predicted above has been found in a numerical simulation of the unrolling of DNA from the histone core, which was performed in a recent application of BD (Klenin and Langowski, manuscript in preparation). A 200 bp DNA was represented as a wormlike chain as before, and attached to the surface of a cylinder 5 nm thick and 6 nm in diameter, assuming a binding energy of 2 kT per base pair, which was distributed uniformly along the contour of the DNA. This surface binding energy, for technical reasons even larger than that estimated in the analytical theory, is largely sufficient to overcome the elastic energy estimated from the persistence length (58 k_BT).

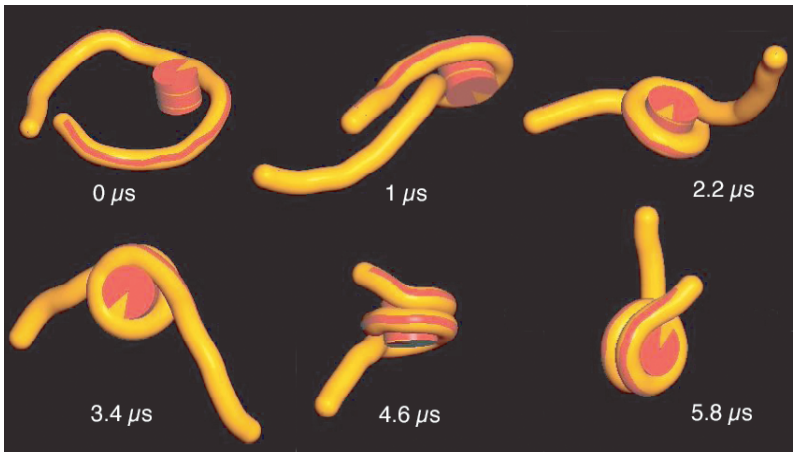

Fig. 5a: BD simulation of wrapping of a 200 bp DNA on the histone core.

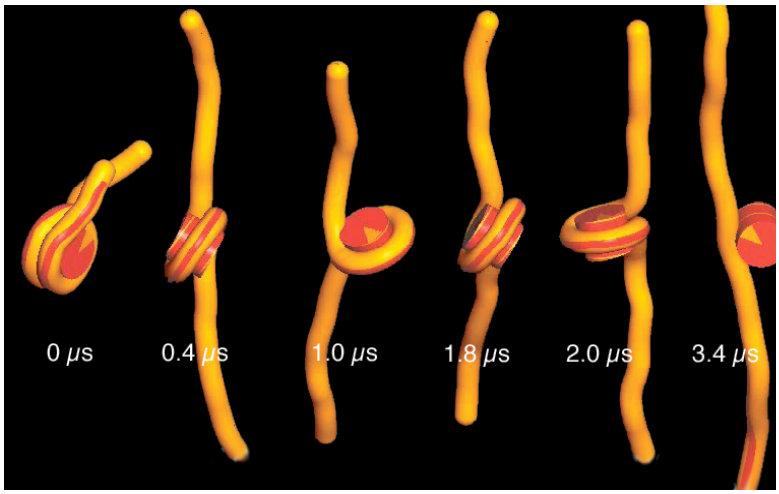

Fig. 5b: BD simulation of unrolling of a 200 bp DNA from the histone core, using a stretching force of 16 pN.

Fig. 5a shows a trajectory from a BD simulation of the wrapping of the DNA on the histone core. Initially, the DNA is bound to one point on the histone octamer surface and then allowed to equilibrate. It is seen that under these conditions the DNA forms a superhelix on the cylinder surface within a few microseconds, the free linker DNA arms diverging slightly from the nucleosome surface (as earlier shown experimentally by Tóth et al. [68]).

Applying a stretching force of 16 pN to the DNA ends leads to unwrapping of the DNA (Fig. 5b). It is remarkable that the unwinding of the first turn is quite fast (0.4 μs), after which a barrier has to be overcome by twisting the nucleosome cylinder (1.8 to 2 μs). Only after this twisting transition has been made, the second turn can unwind, which again is analogous to the arrest of nucleosome unrolling as observed in the single molecule stretching experiments by Brower-Toland et al.[65]. The simulation also shows that the first turn is unrolled significantly faster than the second.

4.4 A possible mechanism for nucleosome unwrapping

The results of the analytical and numerical models agree well. The unwrapping experiment to which we compare them[65] utilized dynamical force spectroscopy (DFS) and exposed the nucleosomal array to a force F increasing at constant rate r_F, $F = r_F t$, and determined the most probable rupture force F^* as a function of loading rate. The rate of unwrapping is expected to be proportional to the Kramers' rate $\exp(\Delta U - \pi R(F_{crit}' - F'))$ from which it can be shown that $F^* \propto \ln(r_F) + const$.

A detailed analysis shows that the rates over the barrier are much too fast in the model as compared to the rates at which nucleosomes unwrap in the experiment[66]. This forced us to critically reconsider the assumptions on which the model was based, especially the – at first sight – straightforward assumption that the adsorption energy per length is constant along the wrapping path. But this neglects an important feature of the nucleosome, namely that the two DNA turns interact. Clearly the turns are close enough to feel a considerable electrostatic repulsion, the exact amount of which is hard to be determined, e.g. due to the fact that the DNA is adsorbed on the low-dielectric protein core (image effects). Moreover, the presence of histone tails complicate things. It is known (see Section 5.2) that the tails adsorb on the nucleosomal DNA. If the nucleosome is fully wrapped the two turns have to share the cationic tails but if there is only one turn left, all these tails can in principle adsorb on this remaining turn. All these effects go in one direction: A remaining DNA turn on the wrapped nucleosome is much stronger adsorbed then a turn in the presence of the second turn wrapped. Indeed, very recent data by the same experimental group show that the force peeks of the discontinuous unwrapping events shift to substantially smaller

values when the tail are partly removed or their charges partially neutralized[69].

The crucial point is now that the adsorption energy k^a was estimated from spontaneous unwrapping events of the second turn in the presence of the other turn [62,63] and thus k^a might have been strongly underestimated since the $k^a = 2k_BT/nm$ include the unfavorable repulsion from the other turn. To account for this we assumed that there is a different effective value of k^a for $\alpha > 0$ (less than one DNA turn) and for $\alpha < 0$ (more than one turn) [66]. Since the discontinuous unwrapping events observed in the experiment clearly correspond to the case where the last term is unwrapped (i.e. to the case $\alpha > 0$) we tuned the parameter k^a such that we can reproduce the DFS data in a satisfying way. From this we found that a value of $k^a = 3.0 - 3.5k_BT/nm$ leads to a good agreement with the experimental data, a value that is *considerably* higher than the effective adsorption energy $k^a = 2k_BT/nm$ felt when a turn is unpeeled in the presence of the other turn.

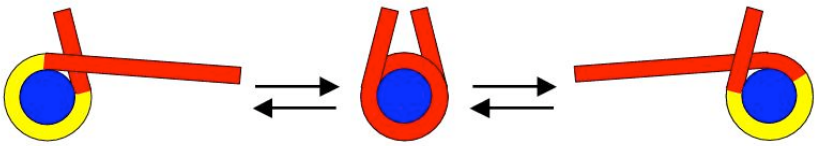

Figure 6. The site exposure mechanism allows access to DNA via spontaneous unwrapping[62,63]. The remaining turn (shown in yellow) has a stronger grip on the octamer and further unpeeling becomes too costly (first-second round difference[66]; see text for details).

This result might explain how the nucleosome can be transparent to DNA binding proteins and at the same time stable. When the nucleosome is fully wrapped each of two turns can easily unwrap spontaneously due to thermal fluctuations and therefore all DNA is transiently accessible for DNA binding proteins, cf. Fig. 6. This has been proven experimentally via competitive protein binding by Widom and coworkers and has been termed the site exposure mechanism[62,63]; recently single molecule fluorescence resonance energy transfer measurements provide additional and more direct evidence for such conformational fluctuations[70,71]. What is, however, puzzling in this set of experiments is why the DNA stops to unpeel further once it encounters the dyad and why it does not fall apart. Our interpretation of the unwrapping data suggests that the reason for this is the first-second round difference as supported by the model calculations. Further simulations using the BD model will be used in the future to test this hypothesis and quantify its consequences.

5. COARSE-GRAINED MODELS OF CHROMATIN

The next higher order structure into which DNA is packed in the eukaryotic nucleus, the chromatin fiber, can again be approximated by a flexible polymer chain. At physiological salt concentrations, this structure has a diameter of 30 nm and a linear mass density of about 5-6 nucleosomes per 10 nm fiber length, corresponding to approx. 100-120 base pairs / nm. Thus, the DNA is compacted by about a factor of 30-40 compared to the 3 base pairs / nm for the canonical B-DNA structure. As mentioned in the Introduction the internal geometry of this structure is still under discussion with more and more experimental evidence for the zig-zag geometry.

The interaction between nucleosomes plays an important role for the stability of the 30 nm fiber; recent experiments on liquid crystals of mononucleosomes [72-75] and also less concentrated mononucleosome solutions [76,77] show an attractive interaction that can be parameterized by an anisotropic Lennard-Jones type potential [20]. Also, an electrostatic interaction potential has been computed using the crystallographic structure of the nucleosome [78]. A recent study[79] investigates the influence of tail bridging on internucleosome interaction (see below).

5.1 Persistence length of chromatin

For the chromatin fiber, estimates of L_p are controversial. Experimental, theoretical and simulation data support values over a wide range starting from L_p = 30-50 nm from scanning force microscopy (SFM) analysis of end-to-end distances of chromatin fibers on mica surface [80]. However, persistence lengths measured by SFM strongly depend on the binding conditions of the fiber to the mica [81]. Stretching chromatin fibers at low salt concentrations with optical tweezers suggests L_p = 30 nm [67], however, chromatin is known to form a very open structure at low salt. Small persistence lengths of 30–50 nm were also postulated from recombination frequencies in human cells [82] and formaldehyde cross-linking probabilities in yeast [83]. These data, however, are strongly influenced by the constraining of the chromatin chain inside a finite nuclear volume; also, the persistence length estimated from looping probabilities depends on the packing density, so these two parameters cannot be determined independently.

Other groups report stiffer fibers with L_p in the range of 100-200 nm, based on distance distributions for genetic marker pairs in human fibroblast nuclei [84-86] or recent experiments in budding yeast using in situ hybridization and live imaging techniques [87]. Stiffer fibers in the range of 200-250 nm are also supported by computer simulations by Mergell et al. [19].

Bystricky et al. [87] determined the persistence length and packing density of yeast chromatin independently by measuring the spatial distance between genetic markers both in fixed cells and *in vivo*. In the equation for the end-to-end distance of a wormlike chain with persistence length L_p,

$$\left\langle r^2 \right\rangle = 2L_p^2\left(L_c/L_p - 1 + e^{-L_c/L_p}\right) \qquad (14)$$

the contour length L_c (in nm) is the ratio of the genomic distance d (in kb) divided by the linear mass density of the chromatin chain c (in bp/nm) or L_c = d/c. A fit of eq. 14 to the values of d and r from the distance measurements yields values for the persistence length L_p = 183 ± 76 nm, and mass density c = 142 ± 21 bp/nm.

Recent experiments [65,67,88-90] investigated the mechanical properties of the chromatin fiber by single molecule stretching techniques. For forces below 10-20 pN, the extension of the chromatin chain is defined by its elasticity and no structural transition occurs, whereas forces above 10-20 pN lead to the disintegration of nucleosomes. Nevertheless quantities like the stretching modulus of a chromatin fiber are still unclear. Stretching a nucleosome-assembled lambda-phage DNA extract with an optical tweezers, Bennink et al. [88] derived a stretching modulus of 150 pN for a salt concentration of 150 mM NaCl.

5.2 Tail bridging for nucleosome attraction

Recent experiments point towards histone tail bridging as a simple mechanism for nucleosomal attraction[76,77,91]. The cationic histone tails extend considerably outside the globular part of the nucleosome as sketched schematically in Fig. 3. Mangenot et al. [76] studied dilute solutions of NCPs by small angle X-ray scattering and suggested that the tails are the main elements responsible for the attraction (which is supported by the fact that the attraction disappears once the tails are removed[91]).

Strong theoretical support that tails are important in the interaction of nucleosomes within a chromatin fiber comes from a very recent computer simulation[17] where the NCP crystal structure has been mimicked by a cylinder with 277 charge patches (accounting for charged groups on the surface of the NCP) with all the tails anchored to it. By switching on and off the charges on the tails it was found that the tails play a crucial role in the electrostatic nucleosome-nucleosome and nucleosome-linker DNA interaction within that chromatin fiber model – especially leading to a stabilization of the fiber at physiological salt conditions. Even though this study shows the importance of tails for nucleosomal interaction, it does not reveal what is really the underlying physical mechanism.

In a recent study[79] we introduced a minimal model for an NCP with tails to test whether such a model shows similar features as the ones found for NCPs. Our NCP model, termed the eight-tail colloid, consists of a sphere with eight attached polymer chains (cf. inset of Fig. 7). The sphere is a very coarse-grained representation of the NCP without the tails, i.e., the globular protein core with the DNA wrapped around. The sphere carries a central charge Z that represents the net charge of the DNA-octamer complex; since the DNA overcharges the cationic protein core, one has $Z < 0$ [64]. The eight histone tails are modelled by flexible, positively charged chains grafted onto the sphere. All parameters in the model have been chosen to match closely the values of the NCP. All charged monomers and the central sphere experience an electrostatic interaction via the standard Debye-Hückel interaction (cf. also Eq. 5).

We demonstrated via BD simulation of a single eight-tail colloid [79] that a single colloid shows indeed similar features as the NCP, especially for small κ the tails are condensed onto the sphere and by increasing the screening the chains desorb. We then determined the interaction between two such complexes and found an attractive pair potential with a minimum of a few $k_B T$. The depth of the potential showed a non-monotonic dependence on the salt concentration which in turn was reflected in a non-monotonic dependence of the second virial coefficient A_2 with a minimum around conditions where the tails unfold. Again, all these observations are qualitatively similar to the experimental ones [76].

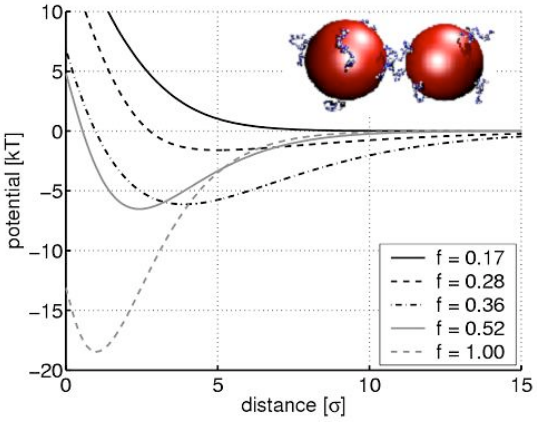

Figure 7. NCP-interaction potential with the NCPs represented by eight-tail colloids (inset); σ = 3.5 Å. Note the strong dependence of the potential depth on the charge fraction of the tail monomers (see [79] for details).

Most importantly, the interaction potential shows a strong dependence on the fraction of charged monomers in the tails, cf. Fig. 7. Starting from a fraction *f* of 0.36 we find a depth of the potential of about 6 k_BT that nearly disappears when *f* is reduced to 0.28. This suggests that the tail bridging can be used by the cellular machinery to control DNA compaction and genetic activity. It is in fact known that the cellular machinery is capable of controlling the charge state of the histone tails via the acetylation (the "discharging") and deacetylation (the "charging") of its lysine groups. Active, acetylated regions in chromatin are more open, inactive, deacetylated regions tend to condense locally and on larger scales as well [92]. For instance, chromatin fibers tend to form hairpin configurations once a sufficiently strong internucleosomal attraction has been reached [19,93]. This suggests a biochemical means by which the degree of chromatin compaction and genetic activity can be controlled via a physical mechanism, the tail-bridging effect.

5.3 Simulation of chromatin fiber stretching

In the low-force regime, nucleosome unrolling does not play a significant role in the dynamics of the chromatin fiber, thus the nucleosome can be simply modeled as a rigid cylinder. In a recent study (Aumann et al. (2005) manuscript submitted) we simulated the stretching of 100-nucleosome chromatin fibers using our earlier Monte-Carlo model [20] and extracted the nanomechanical parameters of the 30 nm fiber from these simulations. The geometry used in these simulations is essentially the 'two-angle' model as described above. The chromatin fiber is approximated as a flexible polymer chain consisting of rigid ellipsoidal disks, 11 nm in diameter and 5.5 nm in height. Internucleosomal interactions are approximated by a more simple potential function than that discussed in the previous section: their attraction is modeled by an anisotropic Lennard-Jones type potential whose depth and minimum position depend on the relative orientation of the two nucleosoms (Gay-Berne-Potential). The disks are connected by linker DNA, which is represented by two cylindrical segments. Incoming and outgoing linker DNA are set 3.1 nm apart vertically on the NCP surface. The length of the linker DNA depends on the presence of linker histones and on the repeat length, which varies from organism to organism [94]. To explore the influence of the linker histone [12], simulations were performed with and without a stem motif added to each nucleosome. To simulate the stretching of the fiber, we added a pulling energy term E_{pull} to the total energy of the conformations during the MC steps, which is proportional to the x-component of the distance between the first and the last nucleosome of the fiber,

$E_{pull} = -M \cdot |\vec{r}_{1,x} - \vec{r}_{N,x}|$, where M is the stretching modulus and $\vec{r}_{i,x}$ is the x-component of the position vector of nucleosome i.

Chains of 100 nucleosomes were simulated using 'pivot' Monte-Carlo moves where parts of the chain were rotated with respect to each other. As in our previous simulations [20], the linker DNA entry-exit angle α was taken as 26° for the initial conformation. This value converges to an effective angle α_{sim} in the range of experimental values between 35° and 45° [12] due to the electrostatic forces and thermal fluctuations. Simulations were done with either a condensed fiber as a starting conformation or an initial conformation where all segments are ordered in a straight line.

To check the statistics of the simulations, we calculated the autocorrelation function $G(\Delta N) = \langle X(N)X(N+\Delta N)\rangle / \langle X(N)\rangle$, where N is the Monte Carlo step number and X either the energy, end-to-end distance or mass density of the fiber conformation at step N. ΔN is the number of steps

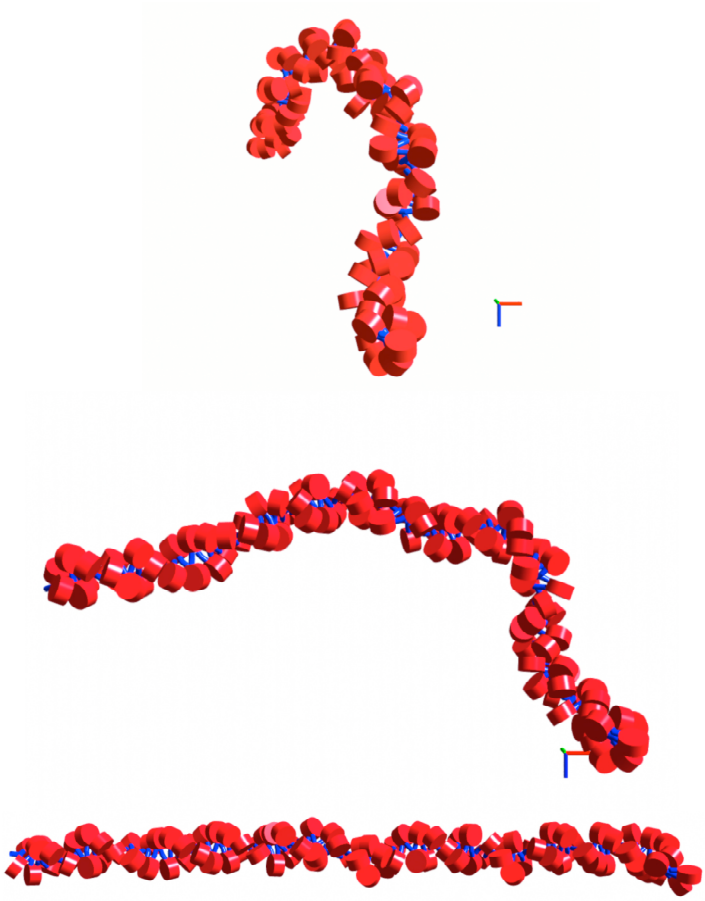

Fig. 8: Stretching simulation of a fiber consisting of 100 nucleosomes (red), linker segments (blue) of repeat length l = 205 nm, an opening angle α_{init}=26° and a twisting angle β=90°. Top is a typical example of an equilibrated structure. Then the fiber is extended by applying an external pulling force F_{pull} = 5 pN and further equilibration initiated (center and bottom).

separating two conformations, and the angular brackets denote the average over the complete trajectory. During the MC procedure, G(ΔN) decreases exponentially with a typical 'correlation length' N_{corr}. We considered two conformations statistically independent if they were separated by at least N_{corr} steps on the trajectory. For the relaxation of the total energy of both systems, we found a maximum of $N_{corr} \approx 3600$ MC steps, for the end to end distance $N_{corr} \approx 3200$ and for the mass density $N_{corr} \approx 2600$. Thus, we performed $5 \cdot 10^5$ MC steps for the initial relaxation of the chain corresponding to more than 100 statistically independent conformations. After the equilibration the stretching potential was switched on and at least 3.10^6 MC steps were performed. For the final analysis, every 1000th conformation was used. Typical fiber conformations during the simulation are shown in Fig. 8.

The bending and stretching rigidities of the modeled chromatin fiber are computed from the trajectories from the fluctuations in the bending angle or the fluctuation in the overall fiber length, respectively. The results show that the bending and the stretching stiffness of the chromatin fiber strongly depend on the local geometry of the nucleosome. Both the persistence length L_p , characterizing the bending stiffness of the fiber, and the stretching modulus ε, which describes the stretching stiffness of the fiber, decrease if either the linker lengths or the opening angle are increased, or the twisting

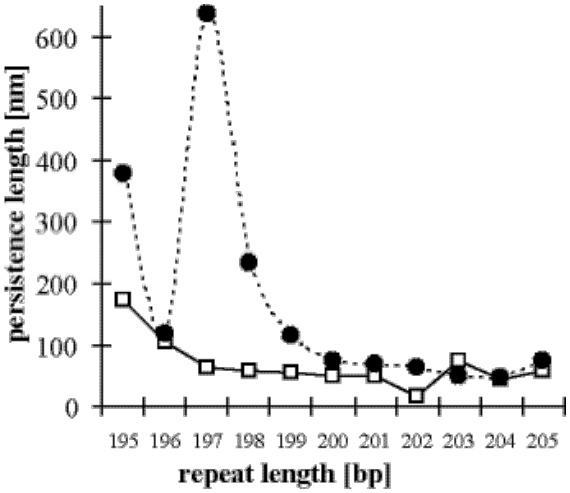

Figure 9: Persistence length of modeled 30 nm chromatin fibers with different nucleosomal repeats in the presence and absence of linker histone H1. The twisting angle between adjacent nucleosomes is adjusted to the canonical value of 360° per 10.5 bp. The persistence lengths of fibers with linker histone (closed symbols, dashed lines) are higher than for fibers without linker histone (open symbols, solid lines). This effect is stronger for short repeats and weakens with increasing repeat length. The peaks show that the twisting angle strongly influences the stiffness of the fiber, leading to a non-monotonous variation of L_p with nucleosome repeat.

angle is reduced. This behavior is independent of the presence of the linker histone H1. The latter decreases the opening angle α between the entry and exit of the linker DNA and as a result leads to a more condensed fiber structure for high salt concentrations[95]. This is in agreement with our simulations since the presence of the linker histone-induced stem motif yields higher persistence lengths thus stiffer fibers (Fig. 9).

The other major result of the simulation comes from comparing the persistence length of the modeled fibers to that of a hypothetical rod from a isotropic elastic material having the same stretching rigidity as the chromatin fiber. Such a rod would have a bending rigidity 4-10 times higher than that actually measured, or simulated here. Thus, the chromatin fiber is less resistant to bending than to stretching. This property of the chromatin fiber is important for its ability to condense and decondense, for example to prevent or allow transcriptional access. Chromatin fibers thus seem to be packed more easily via dense loops than by a linear compression. The formation of hairpin structures has been observed in cryo-EM pictures under the presence of MENT, a heterochromatin protein that mediates higher order chromatin folding [93]. Some hairpin conformations could also be seen in simulations especially for higher internucleosomal attractions [96].

Double-stranded DNA is different from chromatin as far as the ratio of stretching and bending elasticity is concerned [97]: The stretching modulus ε of dsDNA for physiological salt conditions is estimated to ~1100 pN [33,98]. Assuming a homogenous elastic rod with a radius of 1 nm for DNA yields a bending persistence length of L_p = 70 nm, which is only a factor of 1.4 higher then the persistence length of 50 nm for dsDNA; thus, dsDNA is almost equally resistant to stretching and to bending.

As mentioned before, the exact value for the persistence length of the chromatin fiber is still under discussion, with estimates ranging from 30 nm to 260 nm. Some of the small values in this range were obtained at low salt concentrations, where a smaller persistence length compared to our results for high salt can be expected, since low salt is known to open the fiber. Other experiments resulting in small persistence lengths were done in constrained volumes by cross-linking procedures [82,83]. Under these circumstances, the condition of an unconstrained self-crossing walk is only fulfilled over short distances. Thus, for a given chain flexibility, the measured apparent persistence length will depend on the genomic separation and folding topology for which it is calculated[87]. The effect of spatial confinement on the apparent persistence length of a chromatin chain is further elaborated in a recent publication[99]. Furthermore, a persistence length in the range of the

fiber diameter of 30 nm would lead to extremely irregular structures, which are hard to be reconciled with the concept of a "fiber".

Analysis of the distance distribution for genetic marker pairs in human fibroblast nuclei [84-86] provide higher values of L_p = 100-140 nm based on a wormlike chain model. Recent experiments in budding yeast using optimized *in situ* hybridization and live imaging techniques[87] report stiff interphase chromatin fibers estimating a persistence length of 120-200 nm. The persistence lengths that we obtain from the MC simulations for linker lengths of 10 and 15 bp are in the range 50-280 nm, decreasing with longer linkers.

Bennink et. al. derived 150 pN as stretching modulus for a salt concentration of 150 mM NaCl [88], using optical tweezers for the stretching of a nucleosome-assembled lambda-phage DNA extract of a *Xenopus laevis* egg with no linker histones attached and nucleosome repeat length of 200 bp. Our simulations yield a lower value of 40 pN already for a repeat length of 192 (no linker histone). One reason for this discrepancy may be the difference of 50 mM in the salt concentrations, since our simulation parameters have been calibrated for 100 mM NaCl. A lower salt concentration leads to a lower compaction thus to a lower stretching modulus. Furthermore the solution used in the tweezers experiment contains proteins known to act close to the entry-exit points similar to the linker histones. This is supported by the Monte-Carlo simulations, which for a repeat length of 200 bp (with stem) yields a stretching modulus in the range of 90-160 pN. Nevertheless the Gay-Berne potential used in the MC model is only an approximation of the nucleosome-nucleosome interaction, which is strongly dependent on salt conditions. To improve the quantitative predictions of our model, more detailed interaction potentials are need, as for instance the tail-bridging interaction outlined here. Moreover, for the modeling of nucleosome unwrapping and interpreting corresponding experiments[65,88], the DNA – nucleosome interaction has a decisive role. Inclusion of such potentials into the chromatin fiber model will provide a deeper insight in the architecture and behavior of the chromatin fiber as it undergoes biologically important modifications, as well as into its role in transcription and gene regulation.

6. REFERENCES

1. Luger, K., Mäder, A. W., Richmond, R. K., Sargent, D. F. & Richmond, T. J. (1997). Crystal structure of the nucleosome core particle at 2.8 Å resolution. *Nature* **389**, 251-260.

2. Davey, C. A., Sargent, D. F., Luger, K., Maeder, A. W. & Richmond, T. J. (2002). Solvent mediated interactions in the structure of the nucleosome core particle at 1.9 a resolution. *J Mol Biol* **319**, 1097-113.
3. Richmond, T. J. & Davey, C. A. (2003). The structure of DNA in the nucleosome core. *Nature* **423**, 145-50.
4. Schalch, T., Duda, S., Sargent, D. F. & Richmond, T. J. (2005). X-ray structure of a tetranucleosome and its implications for the chromatin fibre. *Nature* **436**, 138-41.
5. Finch, J. T. & Klug, A. (1976). Solenoidal model for superstructure in chromatin. *Proc Natl Acad Sci USA* **73**, 1897-1901.
6. Thoma, F., Koller, T. & Klug, A. (1979). Involvement of histone H1 in the organization of the nucleosome and of the salt-dependent superstructures of chromatin. *J Cell Biol* **83**, 403-27.
7. Widom, J. & Klug, A. (1985). Structure of the 300A chromatin filament: X-ray diffraction from oriented samples. *Cell* **43**, 207-13.
8. Woodcock, C. L., Grigoryev, S. A., Horowitz, R. A. & Whitaker, N. (1993). A chromatin folding model that incorporates linker variability generates fibers resembling the native structures. *Proc Natl Acad Sci USA* **90**, 9021-9025.
9. Horowitz, R. A., Agard, D. A., Sedat, J. W. & Woodcock, C. L. (1994). The three-dimensional architecture of chromatin in situ: electron tomography reveals fibers composed of a continuously variable zig-zag nucleosomal ribbon. *J Cell Biol* 125, 1-10.
10. Woodcock, C. L. & Dimitrov, S. (2001). Higher-order structure of chromatin and chromosomes. *Curr Opin Genet Dev* 11, 130-5.
11. Leuba, S. H., Yang, G., Robert, C., Samori, B., van Holde, K., Zlatanova, J. & Bustamante, C. (1994). Three-dimensional structure of extended chromatin fibers as revealed by tapping-mode scanning force microscopy. *Proc Natl Acad Sci USA* **91**, 11621-11625.
12. Bednar, J., Horowitz, R. A., Grigoryev, S. A., Carruthers, L. M., Hansen, J. C., Koster, A. J. & Woodcock, C. L. (1998). Nucleosomes, linker DNA, and linker histone form a unique structural motif that directs the higher-order folding and compaction of chromatin. *Proc Natl Acad Sci USA* **95**, 14173-14178.
13. Schiessel, H., Gelbart, W. M. & Bruinsma, R. (2001). DNA folding: Structural and mechanical properties of the two- angle model for chromatin. *Biophys J* **80**, 1940-1956.
14. Friedland, W., Jacob, P., Paretzke, H. G. & Stork, T. (1998). Monte Carlo simulation of the production of short DNA fragments by low-linear energy transfer radiation using higher-order DNA models. *Radiation Research* **150**, 170-182.
15. Rydberg, B., Holley, W. R., Mian, I. S. & Chatterjee, A. (1998). Chromatin Conformation in Living Cells: Support for a Zig-Zag Model of the 30 nm Chromatin Fiber. *J Mol Biol* **284**, 71-84.
16. Dorigo, B., Schalch, T., Kulangara, A., Duda, S., Schroeder, R. R. & Richmond, T. J. (2004). Nucleosome arrays reveal the two-start organization of the chromatin fiber. *Science* 306, 1571-3.
17. Sun, J., Zhang, Q. & Schlick, T. (2005). Electrostatic mechanism of nucleosomal array folding revealed by computer simulation. *Proc Natl Acad Sci U S A* **102**, 8180-5.

18. Barbi, M., Mozziconacci, J. & Victor, J. M. (2005). How the chromatin fiber deals with topological constraints. *Phys Rev E Stat Nonlin Soft Matter Phys* **71**, 031910.
19. Mergell, B., Everaers, R. & Schiessel, H. (2004). Nucleosome interactions in chromatin: fiber stiffening and hairpin formation. *Phys Rev E Stat Nonlin Soft Matter Phys* **70**, 011915.
20. Wedemann, G. & Langowski, J. (2002). Computer simulation of the 30-nanometer chromatin fiber. *Biophys J* **82**, 2847-59.
21. Beard, D. A. & Schlick, T. (2001). Computational Modeling Predicts the Structure and Dynamics of Chromatin Fiber. *Structure* 9, 105-114.
22. Katritch, V., Bustamante, C. & Olson, V. K. (2000). Pulling chromatin fibers: Computer simulations of direct physical micromanipulations. *J Mol Biol* **295**, 29-40.
23. Ehrlich, L., Munkel, C., Chirico, G. & Langowski, J. (1997). A Brownian dynamics model for the chromatin fiber. *Comput Appl Biosci* **13**, 271-9.
24. Klenin, K., Merlitz, H. & Langowski, J. (1998). A Brownian dynamics program for the simulation of linear and circular DNA and other wormlike chain polyelectrolytes. *Biophys J* **74**, 780-788.
25. Lu, Y., Weers, B. & Stellwagen, N. C. (2001). DNA persistence length revisited. *Biopolymers* **61**, 261-75.
26. Barkley, M. D. & Zimm, B. H. (1979). Theory of twisting and bending of chain macromolecules: analysis of the fluorescence depolarization of DNA. *J Chem Phys* **70**, 2991-3007.
27. Fujimoto, B. S. & Schurr, J. M. (1990). Dependence of the torsional rigidity of DNA on base composition. *Nature* **344**, 175-7.
28. Schurr, J. M., Fujimoto, B. S., Wu, P. & Song, L. (1992). Fluorescence studies of nucleic acids: dynamics, rigidities and structures. In *Topics in Fluorescence Spectroscopy* (Lakowicz, J. R., ed.), Vol. 3, pp. 137-229. Plenum Press, New York.
29. Shore, D. & Baldwin, R. L. (1983). Energetics of DNA twisting. I. Relation between twist and cyclization probability. *J Mol Biol* **179**, 957-981.
30. Horowitz, D. S. & Wang, J. C. (1984). Torsonal Rigidity of DNA and Length Dependence of the Free Energy of DNA Supercoiling. *J. Mol. Biol.* **173**, 75-91.
31. Taylor, W. H. & Hagerman, P. J. (1990). Application of the method of phage T4 DNA ligase-catalyzed ring-closure to the study of DNA structure I.NaCl-dependence of DNA flexibility and helical repeat. *J. Mol. Biol.* **212**, 363-376.
32. Cluzel, P., Lebrun, A., Heller, C., Lavery, R., Viovy, J. L., Chatenay, D. & Caron, F. (1996). DNA - An Extensible Molecule. *Science* **271**, 792-794.
33. Smith, S. B., Cui, Y. & Bustamante, C. (1996). Overstretching B-DNA: the elastic response of individual double-stranded and single-stranded DNA molecules. *Science* **271**, 795-799.
34. Lankas, F., Sponer, J., Hobza, P. & Langowski, J. (2000). Sequence-dependent Elastic Properties of DNA. *J Mol Biol* **299**, 695-709.
35. Lankas, F., Cheatham, I. T., Spackova, N., Hobza, P., Langowski, J. & Sponer, J. (2002). Critical effect of the n2 amino group on structure, dynamics, and elasticity of DNA polypurine tracts. *Biophys J* **82**, 2592-609.
36. Schellman, J. A. & Stigter, D. (1977). Electrical double layer, zeta potential, and electrophoretic charge of double-stranded DNA. *Biopolymers* **16**, 1415-1434.

37. Klenin, K. V., Frank-Kamenetskii, M. D. & Langowski, J. (1995). Modulation of intramolecular interactions in superhelical DNA by curved sequences: a Monte Carlo simulation study. *Biophys J* **68**, 81-88.
38. Delrow, J. J., Gebe, J. A. & Schurr, J. M. (1997). Comparison of hard-cylinder and screened Coulomb interactions in the modeling of supercoiled DNAs. *Biopolymers* **42**, 455-70.
39. Hammermann, M., Brun, N., Klenin, K. V., May, R., Toth, K. & Langowski, J. (1998). Salt-dependent DNA superhelix diameter studied by small angle neutron scattering measurements and Monte Carlo simulations. *Biophys J* **75**, 3057-3063.
40. Rybenkov, V. V., Cozzarelli, N. R. & Vologodskii, A. V. (1993). Probability of DNA knotting and the effective diameter of the DNA double helix. *Proc Natl Acad Sci USA* **90**, 5307-5311.
41. Rybenkov, V. V., Vologodskii, A. V. & Cozzarelli, N. R. (1997). The effect of ionic conditions on DNA helical repeat, effective diameter and free energy of supercoiling. *Nucl Acids Res* **25**, 1412-1418.
42. Hammermann, M., Steinmaier, C., Merlitz, H., Kapp, U., Waldeck, W., Chirico, G. & Langowski, J. (1997). Salt effects on the structure and internal dynamics of superhelical DNAs studied by light scattering and Brownian dynamics. *Biophys J* **73**, 2674-87.
43. Merlitz, H., Rippe, K., Klenin, K. V. & Langowski, J. (1998). Looping dynamics of linear DNA molecules and the effect of DNA curvature: a study by Brownian dynamics simulation. *Biophys J* **74**, 773-779.
44. Langowski, J., Olson, W. K., Pedersen, S. C., Tobias, I., Westcott, T. P. & Yang, Y. (1996). DNA supercoiling, localized bending and thermal fluctuations. *Trends Biochem Sci* **21**, 50.
45. Metropolis, N., Rosenbluth, A. W., Rosenbluth, M. N., Teller, A. H. & Teller, E. (1953). Equation of state calculations by fast computing machines. *The Journal of Chemical Physics* **21**, 1087-1092.
46. Gebe, J. A. & Schurr, J. M. (1994). Monte-Carlo Simulation of Circular DNAs - 1st Transition in Writhe and Twist Energy Parameters. *Biophys J* **66**, A156-A156.
47. Ermak, D. L. & McCammon, J. A. (1978). Brownian dynamics with hydrodynamic interactions. *J Chem Phys* **69**, 1352-1359.
48. Allison, S. A. (1986). Brownian dynamics simulation of wormlike chains. Fluorescence depolarization and depolarized light scattering. *Macromolecules* **19**, 118-124.
49. Allison, S. A., Sorlie, S. S. & Pecora, R. (1990). Brownian dynamics simulations of wormlike chains: Dynamic light scattering from a 2311 base pair DNA fragment. *Macromolecules* **23**, 1110-1118.
50. Chirico, G. & Langowski, J. (1992). Calculating hydrodynamic properties of DNA through a second-order Brownian dynamics algorithm. *Macromolecules* **25**, 769-775.
51. Allison, S. A., Austin, R. & Hogan, M. (1989). Bending and Twisting Dynamics of Short Linear DNAs - Analysis of the Triplet Anisotropy Decay of a 209-Base Pair Fragment by Brownian Simulation. *J Chem Phys* **90**, 3843-3854.
52. Chirico, G. & Langowski, J. (1994). Kinetics of DNA supercoiling studied by Brownian dynamics simulation. *Biopolymers* **34**, 415-433.

53. Wedemann, G., Munkel, C., Schoppe, G. & Langowski, J. (1998). Kinetics of structural changes in superhelical DNA. *Phys Rev E* **58**, 3537-3546.
54. Bussiek, M., Klenin, K. & Langowski, J. (2002). Kinetics of site-site interactions in supercoiled DNA with bent sequences. *J Mol Biol* **322**, 707-18.
55. Klenin, K. V. & Langowski, J. (2004). Modeling of intramolecular reactions of polymers: an efficient method based on Brownian dynamics simulations. *J Chem Phys* **121**, 4951-60.
56. Klenin, K. V. & Langowski, J. (2001). Diffusion-Controlled Intrachain Reactions of Supercoiled DNA: Brownian Dynamics Simulations. *Biophys. J.* **80**, 69-74.
57. Klenin, K. V. & Langowski, J. (2001). Kinetics of intrachain reactions of supercoiled DNA: Theory and numerical modeling. *J Chem Phys* **114**, 5049-5060.
58. Klenin, K. V. & Langowski, J. (2001). Intrachain Reactions of Supercoiled DNA Simulated by Brownian Dynamics. *Biophys. J.* **81**, 1924-1929.
59. Dickinson, E., Allison, S. A. & McCammon, J. A. (1985). *J. Chem. Soc. Faraday Trans. 2* **81**, 591-601.
60. Rotne, J. & Prager, S. (1969). Variational treatment of hydrodynamic interaction in polymers. *J Chem Phys* **50**, 4831-4837.
61. Chirico, G. & Langowski, J. (1996). Brownian dynamics simulations of supercoiled DNA with bent sequences. *Biophys J* **71**, 955-71.
62. Polach, K. J. & Widom, J. (1996). A model for the cooperative binding of eukaryotic regulatory proteins to nucleosomal target sites. *J Mol Biol* **258**, 800-12.
63. Anderson, J. D. & Widom, J. (2000). Sequence and position-dependence of the equilibrium accessibility of nucleosomal DNA target sites. *J Mol Biol* **296**, 979-87.
64. Schiessel, H. (2003). The physics of chromatin. *J Phys Cond Mat* **15**, R699-R774.
65. Brower-Toland, B. D., Smith, C. L., Yeh, R. C., Lis, J. T., Peterson, C. L. & Wang, M. D. (2002). Mechanical disruption of individual nucleosomes reveals a reversible multistage release of DNA. *Proc Natl Acad Sci U S A* **99**, 1960-5.
66. Kulic, I. M. & Schiessel, H. (2004). DNA Spools under Tension. *Phys Rev Lett* **92**, 228101-4.
67. Cui, Y. & Bustamante, C. (2000). Pulling a single chromatin fiber reveals the forces that maintain its higher-order structure. *Proc Natl Acad Sci U S A* **97**, 127-132.
68. Tóth, K., Brun, N. & Langowski, J. (2001). Trajectory of nucleosomal linker DNA studied by fluorescence resonance energy transfer. *Biochemistry* **40**, 6921-6928.
69. Brower-Toland, B., Wacker, D. A., Fulbright, R. M., Lis, J. T., Kraus, W. L. & Wang, M. D. (2005). Specific contributions of histone tails and their acetylation to the mechanical stability of nucleosomes. *J Mol Biol* **346**, 135-46.
70. Li, G., Levitus, M., Bustamante, C. & Widom, J. (2005). Rapid spontaneous accessibility of nucleosomal DNA. *Nat Struct Mol Biol* **12**, 46-53.
71. Tomschik, M., Zheng, H., van Holde, K., Zlatanova, J. & Leuba, S. H. (2005). Fast, long-range, reversible conformational fluctuations in nucleosomes revealed by single-pair fluorescence resonance energy transfer. *Proc Natl Acad Sci U S A* **102**, 3278-83.
72. Leforestier, A. & Livolant, F. (1997). Liquid crystalline ordering of nucleosome core particles under macromolecular crowding conditions: evidence for a discotic columnar hexagonal phase. *Biophys J* **73**, 1771-6.

73. Livolant, F. & Leforestier, A. (2000). Chiral discotic columnar germs of nucleosome core particles. *Biophys J* **78**, 2716-29.
74. Leforestier, A., Dubochet, J. & Livolant, F. (2001). Bilayers of nucleosome core particles. *Biophys J* **81**, 2414-21.
75. Mangenot, S., Leforestier, A., Durand, D. & Livolant, F. (2003). X-ray diffraction characterization of the dense phases formed by nucleosome core particles. *Biophys J* **84**, 2570-84.
76. Mangenot, S., Raspaud, E., Tribet, C., Belloni, L. & Livolant, F. (2002). Interactions between isolated nucleosome core particles: A tail-bridging effect? *Eur Phys J E* **7**, 221-231.
77. Mangenot, S., Leforestier, A., Vachette, P., Durand, D. & Livolant, F. (2002). Salt-induced conformation and interaction changes of nucleosome core particles. *Biophys J* **82**, 345-56.
78. Beard, D. A. & Schlick, T. (2001). Modeling salt-mediated electrostatics of macromolecules: the discrete surface charge optimization algorithm and its application to the nucleosome. *Biopolymers* **58**, 106-15.
79. Muehlbacher, F., Holm, C. & Schiessel, H. (2005). Controlled DNA compaction within chromatin: the tail-bridging effect. *Europhysics Letters, in press*.
80. Castro, C. (1994). Measurement of the elasticity of single chromatin fibers: the effect of histone H1. PhD Thesis, University of Oregon, Eugene.
81. Bussiek, M., Mucke, N. & Langowski, J. (2003). Polylysine-coated mica can be used to observe systematic changes in the supercoiled DNA conformation by scanning force microscopy in solution. *Nucleic Acids Res* **31**, e137.
82. Ringrose, L., Chabanis, S., Angrand, P. O., Woodroofe, C. & Stewart, A. F. (1999). Quantitative comparison of DNA looping *in vitro* and *in vivo*: chromatin increases effective DNA flexibility at short distances. *EMBO J* **18**, 6630-6641.
83. Dekker, J., Rippe, K., Dekker, M. & Kleckner, N. (2002). Capturing Chromosome Conformation. *Science* **295**, 1306-1311.
84. van den Engh, G., Sachs, R. & Trask, B. J. (1992). Estimating genomic distance from DNA sequence location in cell nuclei by a random walk model. *Science* **257**, 1410-1412.
85. Trask, B. J., Allen, S., Massa, H., Fertitta, A., Sachs, R., van den Engh, G. & Wu, M. (1993). Studies of metaphase and interphase chromosomes using fluorescence in situ hybridization. *Cold Spring Harb Symp Quant Biol* **58**, 767-75.
86. Yokota, H., van den Engh, G., Hearst, J., Sachs, R. K. & Trask, B. J. (1995). Evidence for the organization of chromatin in megabase pair-sized loops arranged along a random walk path in the human G0/G1 interphase nucleus. *J Cell Biol* **130**, 1239-1249.
87. Bystricky, K., Heun, P., Gehlen, L., Langowski, J. & Gasser, S. M. (2004). Long-range compaction and flexibility of interphase chromatin in budding yeast analyzed by high-resolution imaging techniques. *Proc Natl Acad Sci U S A* **101**, 16495-500.
88. Bennink, M. L., Leuba, S. H., Leno, G. H., Zlatanova, J., de Grooth, B. G. & Greve, J. (2001). Unfolding individual nucleosomes by stretching single chromatin fibers with optical tweezers. *Nat Struct Biol* **8**, 606-10.
89. Leuba, S. H., Bennink, M. L. & Zlatanova, J. (2004). Single-molecule analysis of chromatin. *Methods Enzymol* **376**, 73-105.

90. Claudet, C., Angelov, D., Bouvet, P., Dimitrov, S. & Bednar, J. (2005). Histone octamer instability under single molecule experiment conditions. *J Biol Chem* **280**, 19958-65.
91. Bertin, A., Leforestier, A., Durand, D. & Livolant, F. (2004). Role of histone tails in the conformation and interactions of nucleosome core particles. *Biochemistry* **43**, 4773-80.
92. Tse, C., Sera, T., Wolffe, A. P. & Hansen, J. C. (1998). Disruption of higher-order folding by core histone acetylation dramatically enhances transcription of nucleosomal arrays by RNA polymerase III. *Mol Cell Biol* **18**, 4629-4638.
93. Grigoryev, S. A., Bednar, J. & Woodcock, C. L. (1999). MENT, a heterochromatin protein that mediates higher order chromatin folding, is a new serpin family member. *J Biol Chem* **274**, 5626-36.
94. van Holde, K. E. (1989). *Chromatin*, Springer, Heidelberg.
95. van Holde, K. & Zlatanova, J. (1996). What determines the folding of the chromatin fiber. *Proceedings of the National Academy of Sciences of the USA* **93**, 10548-10555.
96. Mergell, B., Everaers, R. & Schiessel, H. (2004). Nucleosome interactions in chromatin: fiber stiffening and hairpin formation. *Phys Rev E* **70**, 011915.
97. Bustamante, C., Smith, S. B., Liphardt, J. & Smith, D. (2000). Single-molecule studies of DNA mechanics. *Curr Opin Struct Biol* **10**, 279-85.
98. Baumann, C. G., Smith, S. B., Bloomfield, V. A. & Bustamante, C. (1997). Ionic effects on the elasticity of single DNA molecules. *Proc Natl Acad Sci U S A* **94**, 6185-6190.
99. Gehlen, L. R., Rosa, A., Klenin, K., Langowski, J., Gasser, S. & Bystricky, K. (2005). Spatially confined polymer chains: implication of chromatin fiber flexibility and peripheral anchoring on telomere-telomere interaction. *J Phys Cond Matter,* in press.